KYBERNETIKA — VOLUME 35 (1999), NUMBER 1, PAGES 133 - 146

A CONSERVATIVE SPECTRAL ELEMENT METHOD FOR THE APPROXIMATION OF COMPRESSIBLE FLUID FLOW

KELLY BLACK

A method to approximate the Euler equations is presented. The method is a multi-domain approximation, and a variational form of the Euler equations is found by making use of the divergence theorem. The method is similar to that of the Discontinuous-Galerkin method of Cockburn and Shu, but the implementation is constructed through a spectral, multi-domain approach. The method is introduced and is shown to be a conservative scheme. A numerical example is given for the expanding flow around a point source as a comparison with the method proposed by Kopriva.

1. INTRODUCTION

A multi-domain, spectral method is used to approximate a variational form of the Euler equations. The computational domain is first subdivided into non-overlapping subdomains. By making use of the divergence theorem, the divergence of the flux terms are not calculated. Instead, an area integral of the flux terms is approximated and the boundary integral of the flux approximated making use of upwinding and Gauss quadratures. The method presented here is similar to that of Cockburn and Shu [2, 3, 4]. (The scheme has also been extended to the viscous case [1].)

A relatively small number of multi-domain high-order spectral approximations have been developed to approximate compressible flow. Among them are the those proposed by Hesthaven [8, 9, 10] and Kopriva [11, 12]. The method proposed by Hesthaven is a penalty method employing a Chebychev collocation scheme. A penalty method is employed in which the penalty is enforced on either the viscous or the convective terms depending on the characteristics of the convective operator.

The method proposed by Kopriva [11, 12] is also a Chebychev collocation scheme. Rather than make use of a penalty method, the approximation is constructed on the Chebychev–Gauss abscissa, and the fluxes on the interior are determined by converting between three different grids. In one step, the fluxes are converted to a Gauss/Gauss–Lobatto grid in the x and y-directions and the flux in one direction is averaged across the interface of adjacent subdomains. In the following step, the flux on the remaining faces is approximated in a similar manner.

The scheme proposed here is constructed from a variational method. It has many of the advantages of the other methods, and like the method proposed by Kopriva, the subdomain interfaces are calculated on the Gauss abscissa which effectively ignores the corners of the subdomains and offers more flexibility in how the domain is decomposed into its subdomains. The principle advantage of the method proposed here is the relative simplicity of the algorithm. Their is no grid conversion, and the fluxes at the interfaces are treated like Riemann problems and standard flux splitting schemes can be used to approximate the interface fluxes.

To introduce the method, a brief overview of the discontinuous Galerkin method is presented followed by an introduction into the spectral element implementation of the method. The method is shown to be conservative, and two numerical examples are given. The first is for the flow in an expanding nozzle which is given for a comparison to the method proposed by Kopriva [11]. The second is for flow around a circular cylinder.

2. DISCONTINUOUS GALERKIN METHOD

The basic idea is to express the equation to be approximated as the divergence of fluxes and make use of the divergence theorem to express the discretization with area integrals and surface integrals. We will take advantage of the scheme to approximate the Euler equations of gas dynamics,

$$\boldsymbol{u}_t + \nabla \cdot \langle \boldsymbol{F}, \boldsymbol{G} \rangle = 0, \tag{1}$$

$$\boldsymbol{u} = \begin{bmatrix} \rho \\ \rho u \\ \rho v \\ \rho e \end{bmatrix},$$

$$\boldsymbol{F} = \begin{bmatrix} \rho u \\ p + \rho u^2 \\ \rho uv \\ u(\rho e + p) \end{bmatrix}, \qquad \boldsymbol{G} = \begin{bmatrix} \rho v \\ \rho uv \\ p + \rho v^2 \\ v(\rho e + p) \end{bmatrix},$$

where ρ is the density, u is the velocity in the x-direction, v is the velocity in the y-direction, and e is the specific energy. The pressure, p, is related by the specific and kinetic energy, $p = (\gamma - 1)(\rho e - \frac{\rho}{2}(u^2 + v^2))$, and $\gamma = 1.4$ (a perfect gas is assumed).

The computational domain is separated into subdomains, Ω_k. The union of the subdomains, $\cup_k \Omega_k$, is the full computational domain, and the subdomains only overlap on their boundaries. The approximation of the state is found through a linear combination of basis functions, $\phi_{ij}(x, y)$, within each subdomain. For example, the approximation for the density,

$$\rho_N(x, y) = \sum_{i=0}^{N_x} \sum_{j=0}^{N_y} \hat{\rho}_{ij} \phi_{ij}(x, y), \tag{2}$$

is determined by finding the coefficients, $\hat{\rho}_{ij}$. The approximation of the state is denoted $\boldsymbol{u}_N$. Since a collocation type spectral element method is implemented, the approximation of the flux is found on the collocation points and is denoted $\langle \boldsymbol{F}_N, \boldsymbol{G}_N \rangle$.

The approximation for the Euler equations is enforced through a variational method, and on each individual subdomain, Ω_k, a variational form is defined:

$$\begin{aligned} & \int\int_{\Omega_k} \frac{\partial}{\partial t} \boldsymbol{u}_N \, \phi_{mn}(x,y) \, \mathrm{d}x\mathrm{d}y \\ & - \int\int_{\Omega_k} \langle \boldsymbol{F}_N, \boldsymbol{G}_N \rangle \cdot \nabla \phi_{mn}(x,y) \, \mathrm{d}x\mathrm{d}y \\ & + \int_{\partial\Omega_k} \langle \boldsymbol{F}_N, \boldsymbol{G}_N \rangle \cdot \vec{n} \, \phi_{mn}(x,y) \, \mathrm{d}s = 0. \end{aligned} \tag{3}$$

The area integrals are approximated by making use of the Legendre–Gauss quadrature, and the approximation of each integral only requires interior points from within each subdomain. The surface integral is approximated by finding the state on either side of each subdomain and making use of a van Leer splitting scheme to approximate the flux for the corresponding Riemann problem.

2.1. Spectral elements

The method proposed is essentially a spectral-element approximation using the discontinuous Galerkin method. The basis functions are found from the Lagrange polynomial interpolating the abscissa of the Legendre–Gauss quadrature. The method does not make use of the Legendre–Gauss–Lobatto quadrature. Unlike other spectral-element methods, it is a disadvantage to use points on the boundaries of the subdomains to approximate the area integral in equation (3).

The Legendre–Gauss quadrature includes the abscissa, η_i, and the weights, w_i, for $i = 0 \ldots N$ and can be used to calculate the integral of a polynomial up to a given degree, $2N$,

$$\int_{-1}^{1} \Pi_{2N}(\eta) \, \mathrm{d}\eta \;=\; \sum_{i=0}^{N} \Pi_{2N}(\eta_i) \, w_i. \tag{4}$$

The basis functions are defined to be the Lagrange interpolants on the abscissa,

$$\psi_m(\eta_i) \;=\; \delta_{mi}, \quad 0 \le i, \, m \le N, \tag{5}$$

and each basis function is a polynomial of a given degree, N. An important identity which will be used later is that the Lagrange polynomials satisfy

$$\sum_{m=0}^{N} \psi_m(x) \;=\; 1. \tag{6}$$

The basis functions for the two dimensional approximation are found from a tensor product of the interpolants:

$$\phi_{mn}(x,y) \;=\; \psi_m(x) \, \psi_n(y). \tag{7}$$

The approximation is constructed from a linear combination of the Lagrange interpolants. For example, the approximation of the density is

$$\rho_N = \sum_{i=0}^{N_x} \sum_{j=0}^{N_y} \hat{\rho}_{ij} \psi_i(x) \psi_j(y), \tag{8}$$

where the unknowns are the coefficients $\hat{\rho}_{ij}$. Because the basis functions are the Lagrange interpolants, the problem is the same as finding the value of the approximation on the grid points.

2.2. Implementation

The approximation space within a given subdomain is the space of polynomials up to a given degree, and the approximation space is the space of piecewise polynomials. However, the basis functions defined in equation (7) are inadequate for anything other than the square $(\eta, \xi) \in [-1, 1] \times [-1, 1]$.

To overcome this restriction each subdomain is mapped to a square domain, and the approximation is found using the mapping (see Figure 1). Each subdomain must be constructed so that it can be smoothly mapped to a square. The numerical mapping is found using a Gordon–Hall transformation [6]. In particular, each subdomain is mapped to the square via the transformation

$$x = x(\xi, \eta), \quad y = y(\xi, \eta).$$

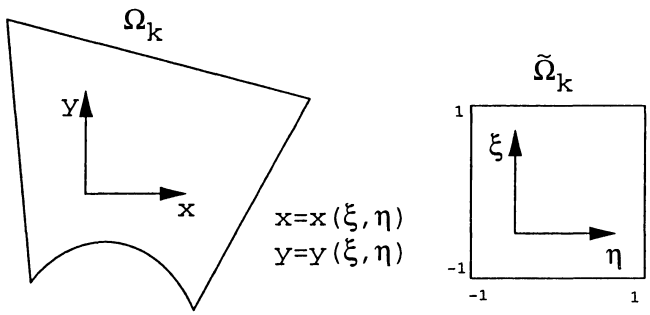

Fig. 1. Curvilinear mapping from a computational subdomain to a square, $(x, y) \in [-1, 1] \times [-1, 1]$.

The variational form of the equation, equation (3), is defined on the original subdomain, Ω_k, and the numerical approximation is found on the transformed subdomain, $\tilde{\Omega}_k$, and the Jacobian of the transformation,

$$J_N = \begin{vmatrix} \frac{\partial x}{\partial \eta} & \frac{\partial x}{\partial \xi} \\ \frac{\partial y}{\partial \eta} & \frac{\partial y}{\partial \xi} \end{vmatrix}, \tag{9}$$

is required. It is assumed that the mapping is a polynomial of the same degree as the approximation, and the Jacobian evaluated at a specific point, (η_i, ξ_j), is denoted

$(J_N)_{ij}$. The discrete divergence operator, ∇_N, must also be defined with respect to the coordinate transformation where

$$\nabla_N \left(\tilde{\psi}_m(\eta)\tilde{\psi}_n(\xi)\right) = \frac{1}{J_N} \begin{bmatrix} \frac{\partial y}{\partial \xi} & -\frac{\partial y}{\partial \eta} \\ -\frac{\partial x}{\partial \xi} & \frac{\partial x}{\partial \eta} \end{bmatrix} \begin{bmatrix} \tilde{\psi}'_m(\eta)\tilde{\psi}_n(\xi)\tilde{\psi}_m(\eta)\tilde{\psi}'_n(\xi) \end{bmatrix}. \tag{10}$$

On a given subdomain, Ω_k, the inner product defined in equation (3) is

$$\begin{aligned} & \int_{\xi=-1}^{1}\int_{\eta=-1}^{1} \frac{\partial}{\partial t}\boldsymbol{u}_N\ \tilde{\psi}_m(\eta)\tilde{\psi}_n(\xi)J_N\,\mathrm{d}\eta\mathrm{d}\xi \qquad (11) \\ = & \int_{\xi=-1}^{1}\int_{\eta=-1}^{1} \langle \boldsymbol{F}_N, \boldsymbol{G}_N\rangle \cdot \nabla_N \left(\tilde{\psi}_m(\eta)\tilde{\psi}_n(\xi)\right) J_N\,\mathrm{d}\eta\mathrm{d}\xi \\ - & \int_{\partial\Omega_k} \langle \boldsymbol{F}_N, \boldsymbol{G}_N\rangle \cdot \vec{n}\ \psi_m(x)\,\psi_n(y)\,\mathrm{d}s. \end{aligned}$$

The left hand side of this equation is approximated using the quadrature which yields

$$\sum_{i=0}^{N_x}\sum_{j=0}^{N_y} \frac{\partial}{\partial t}\,(\boldsymbol{u}_N)_{ij}\,\tilde{\psi}_m(\eta_i)\,\tilde{\psi}_n(\xi_j)\,J_{ij}w_iw_j, \tag{12}$$

where J_{ij} is the Jacobian evaluated at (η_i, ξ_j). The basis functions are the Lagrange interpolants, and the left hand side reduces to

$$\frac{\partial}{\partial t}\,(\boldsymbol{u}_N)_{mn}\,J_{mn}w_mw_n \tag{13}$$

(the mass matrix is diagonal). Likewise, the area integral on the right hand side of equation (11) is found through the use of equation (10) and the quadrature.

The surface integral in equation (11) is approximated by finding the values of the numerical flux on the boundaries, which coincide with the abscissa from the Legendre–Gauss quadrature. The flux is calculated on the interior points of a given domain, the state at the boundaries is found. For example, the density on the bottom boundary, $\xi = -1$, is calculated via

$$\rho_N(s_m, -1) = \sum_{i=0}^{N_x}\sum_{j=0}^{N_y} \hat{\rho}_{ij}\tilde{\psi}_i(s_m)\tilde{\psi}_j(-1) = \sum_{j=0}^{N_y} \hat{\rho}_{mj}\tilde{\psi}_j(-1).$$

Once the state on the boundaries is defined, the flux is calculated using a flux-splitting method [13, 7]. The flux is defined on the abscissa of the Legendre–Gauss quadrature on the boundaries, and the boundary integral can be easily approximated. The abscissa do not include the corners which reduces the constraints on the decomposition into the subdomains. For example, there are no restrictions on having more than four subdomains meet at one corner.

The fluxes are calculated at the boundaries are the same on either side of a subdomain interface, and the resulting scheme is conservative. In particular, the rate

of change of the conserved variable in one domain, Ω_k can be found by integrating over the whole subdomain,

$$\int\int_{\Omega_k} \frac{\partial}{\partial t} \boldsymbol{u}_N \, \mathrm{d}x\mathrm{d}y \;=\; \int\int_{\tilde{\Omega}_k} \frac{\partial}{\partial t} \boldsymbol{u}_N J_N \, \mathrm{d}\eta\mathrm{d}\xi.$$

This can be expressed as a sum of the basis functions since the Lagrange interpolants are used (from equation (6),

$$\sum_{m=0}^{N_x}\sum_{n=0}^{N_y} \int\int_{\Omega_k} \frac{\partial}{\partial t} \boldsymbol{u}_N \tilde{\psi}_m(\eta)\tilde{\psi}_n(\xi) J_N \, \mathrm{d}\eta\mathrm{d}\xi. \tag{14}$$

The integral is approximated by making use of the quadrature which is

$$\sum_{m=0}^{N_x}\sum_{n=0}^{N_y}\sum_{i=0}^{N_x}\sum_{j=0}^{N_y} \left(\frac{\partial}{\partial t}\boldsymbol{u}_N\right) \tilde{\psi}_m(\eta_i)\tilde{\psi}_n(\xi_j)\,(J_N)_{ij}\, w_i w_j. \tag{15}$$

Equation (14) is the left hand side of equation (11) and is the sum over all of the basis functions and represents the rate of change of the conserved quantities. It will be shown that this sum is zero by examining the area integral given in the right hand side of equation (11). The corresponding sum of the discrete approximations on the right hand side of equation (11) is

$$\sum_{m=0}^{N_x}\sum_{n=0}^{N_y}\sum_{i=0}^{N_x}\sum_{j=0}^{N_y} \langle (\boldsymbol{F}_N)_{ij}, (\boldsymbol{G}_N)_{ij} \rangle \cdot \nabla_N \left(\tilde{\psi}_m(\eta)\tilde{\psi}_n(\xi)\right)_{\eta=\eta_i,\ \xi=\xi_j} (J_N)_{ij}\, w_i w_j. \tag{16}$$

The sum can be broken into one part that only includes the flux in the x-direction, $\boldsymbol{F}_N$, and a part that only includes the flux in the y-direction, $\boldsymbol{G}_N$. We will concentrate on the flux in the x-direction and show that its contribution sums to zero:

$$\sum_{m=0}^{N_x}\sum_{n=0}^{N_y}\sum_{i=0}^{N_x}\sum_{j=0}^{N_y} (\boldsymbol{F}_N)_{ij} \left(\tilde{\psi}'_m(\eta_i)\,\tilde{\psi}_n(\xi_j) \left(\frac{\partial y}{\partial \xi}\right)_{ij} - \tilde{\psi}_m(\eta_i)\,\tilde{\psi}'_n(\xi_j) \left(\frac{\partial y}{\partial \eta}\right)_{ij} \right) w_i w_j,$$

where $\left(\frac{\partial y}{\partial \xi}\right)_{ij}$ is the derivative of the mapping evaluated at the point (η_i, ξ_j).

The sums can be divided into two parts which expand to

$$\sum_{m=0}^{N_x}\sum_{n=0}^{N_y}\sum_{i=0}^{N_x}\sum_{j=0}^{N_y} (\boldsymbol{F}_N)_{ij}\, \tilde{\psi}'_m(\eta_i)\,\tilde{\psi}_n(\xi_j) \left(\frac{\partial y}{\partial \xi}\right)_{ij} w_i w_j$$

$$- \sum_{m=0}^{N_x}\sum_{n=0}^{N_y}\sum_{i=0}^{N_x}\sum_{j=0}^{N_y} (\boldsymbol{F}_N)_{ij}\, \tilde{\psi}_m(\eta_i)\,\tilde{\psi}'_n(\xi_j) \left(\frac{\partial y}{\partial \eta}\right)_{ij} w_i w_j,$$

and the sums can be rearranged,

$$\sum_{n=0}^{N_y}\sum_{i=0}^{N_x}\sum_{j=0}^{N_y}\left((\boldsymbol{F}_N)_{ij}\,\tilde{\psi}_n(\xi_j)\left(\frac{\partial y}{\partial \xi}\right)_{ij} w_i w_j \left(\sum_{m=0}^{N_x}\tilde{\psi}'_m(\eta_i)\right)\right) \tag{17}$$
$$-\sum_{m=0}^{N_x}\sum_{i=0}^{N_x}\sum_{j=0}^{N_y}\left((\boldsymbol{F}_N)_{ij}\,\tilde{\psi}_m(\eta_i)\left(\frac{\partial y}{\partial \eta}\right)_{ij} w_i w_j \left(\sum_{n=0}^{N_y}\tilde{\psi}'_n(\xi_j)\right)\right).$$

The derivative within the inner sums can be factored to give

$$\sum_{n=0}^{N_y}\sum_{i=0}^{N_x}\sum_{j=0}^{N_y}\left((\boldsymbol{F}_N)_{ij}\,\tilde{\psi}_n(\xi_j)\left(\frac{\partial y}{\partial \xi}\right)_{ij} w_i w_j \left(\frac{\mathrm{d}}{\mathrm{d}\eta}\sum_{m=0}^{N_x}\tilde{\psi}_m(\eta)\right)_{\eta=\eta_i}\right) \tag{18}$$
$$-\sum_{m=0}^{N_x}\sum_{i=0}^{N_x}\sum_{j=0}^{N_y}\left((\boldsymbol{F}_N)_{ij}\,\tilde{\psi}_m(\eta_i)\left(\frac{\partial y}{\partial \eta}\right)_{ij} w_i w_j \left(\frac{\mathrm{d}}{\mathrm{d}\xi}\sum_{n=0}^{N_y}\tilde{\psi}_n(\xi)\right)_{\xi=\xi_j}\right).$$

The inner sum is a sum of the Lagrange polynomials and can be reduced to

$$\sum_{n=0}^{N_y}\sum_{i=0}^{N_x}\sum_{j=0}^{N_y}\left((\boldsymbol{F}_N)_{ij}\,\tilde{\psi}_n(\xi_j)\left(\frac{\partial y}{\partial \xi}\right)_{ij} w_i w_j \left(\frac{\mathrm{d}}{\mathrm{d}\eta}(1)\right)\right)$$
$$-\sum_{m=0}^{N_x}\sum_{i=0}^{N_x}\sum_{j=0}^{N_y}\left((\boldsymbol{F}_N)_{ij}\,\tilde{\psi}_m(\eta_i)\left(\frac{\partial y}{\partial \eta}\right)_{ij} w_i w_j \left(\frac{\mathrm{d}}{\mathrm{d}\xi}(1)\right)\right),$$

which is zero (from equation (6)). The sums for the flux in the y-direction also sum to zero which can be shown in the same manner.

An upwinding scheme is used to calculate the fluxes at the boundaries, and the flux on either side of a subdomain interface is identical. The only difference between the surface integrals on the interface between two adjacent subdomains is the sign of the normal vector. When the contributions from the boundary integrals are added up over the computational domain, the result sums to zero over the subdomain interfaces leaving only the boundary integrals. The change in the conserved variables given in equation (15) depends only on the boundaries, and the scheme is conservative.

3. NUMERICS

Two numerical trials are examined. The first is the flow within an expanding nozzle and the second is for the flow around a circular cylinder. The first example, the nozzle flow, is used as a comparison to the numerical trials of Kopriva [11, 12]. The second flow is used to demonstrate the method in a domain that is not simply connected.

3.1. Nozzle flow

The domain for the first flow, the nozzle flow, is taken to coincide with an expanding flow from a point source (see Figure 4). The top and bottom sides of the domain are constructed to coincide with streamlines of the flow. The level curves of the density, mach number, and pressure are circles centered at the origin. The true solution for the steady, irrotational flow can be calculated through a Hodograph transformation [5].

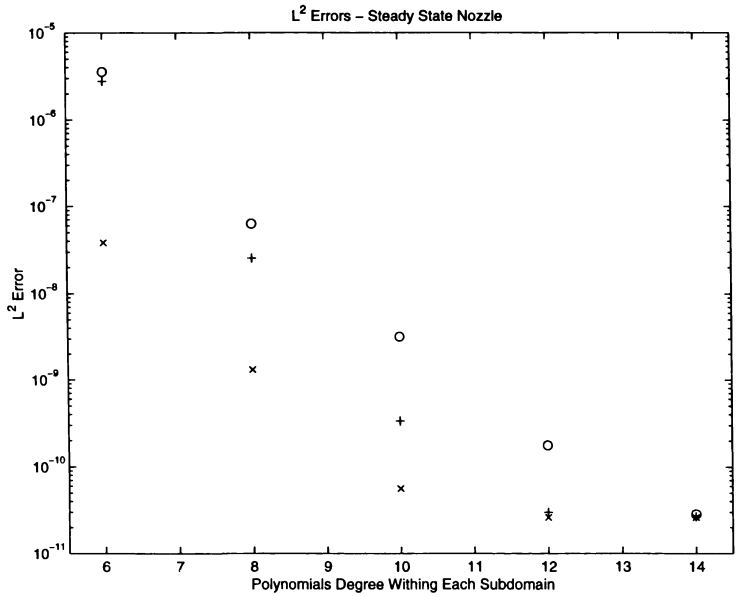

Fig. 2. L^2 errors for the flow within an expanding nozzle. The regular grid is denoted with ×, the bulged grid a +, and the wedged grid an o.

The flow for the nozzle is chosen so that it offers a direct comparison to the example given by Kopriva [11]. The velocity field is chosen so that the mach number at the lower left hand corner is 0.6. The numerical trials, including the geometry, domain decomposition, and boundaries, were chosen based on the trials presented by Kopriva [11], and the domain is subdivided into four curvilinear subdomains. The steady state solution was found using a second order Runga–Kutta method and time marching until the approximation reached a steady state.

Numerical trials were run for three different domain partitions (see Figure 4). The partitions were chosen to be the same as those chosen by Kopriva [12]. The L^2-errors for the approximation are shown in Figures 2 and 3. The rates of convergence are slightly better than that reported by Kopriva [11] using a staggered grid (see Figure 3). However, a larger reduction in accuracy for the deformed grids was found (see Figure 2). Like the results of Kopriva, the rate of convergence for the "Bulged" grid is higher than for the "Regular" grid.

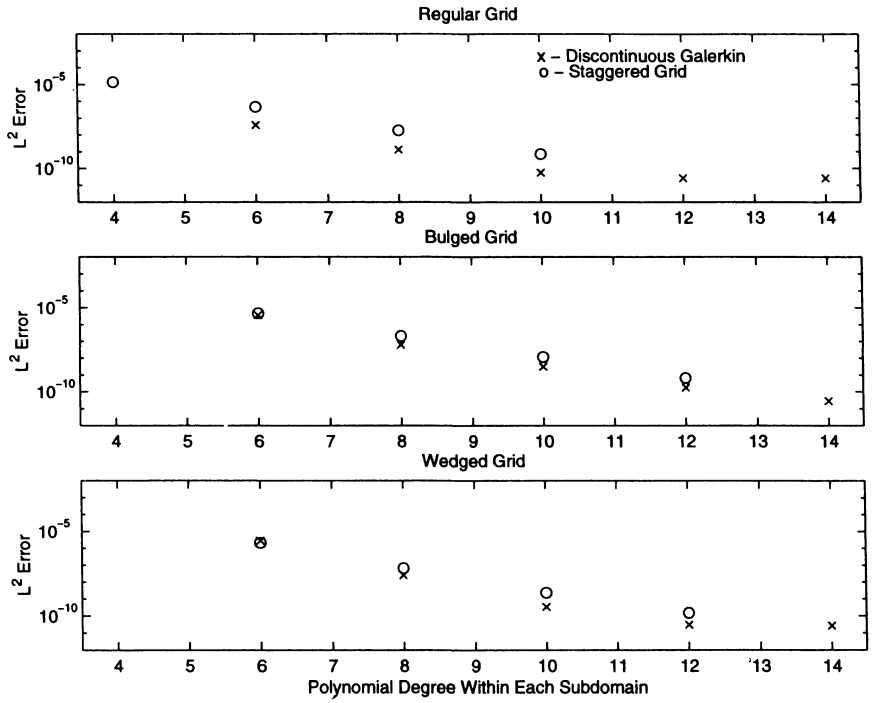

Fig. 3. Comparison between L^2 accuracies of the staggered grid approximation and the discontinuous-Galerkin approximation. (Staggered grid results provided by David Kopriva.)

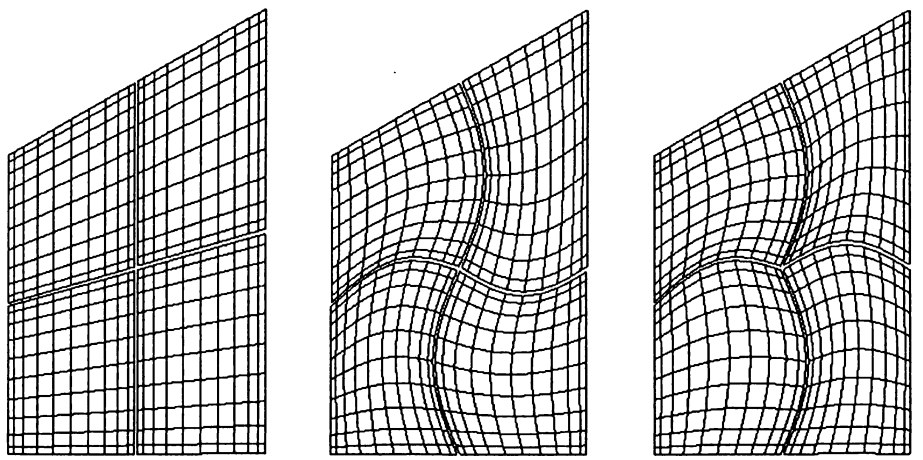

Regular Grid Bulging Grid Wedged Grid

Fig. 4. Mesh used for approximation of flow in an expanding nozzle. The mesh shown is for the Legendre–Gauss abscissa on four subdomains.

3.2. Cylinder Flow

The second set of trials is for the approximation of a flow around a circular cylinder. The parameters used for all of these trials is given in Table 1. Here two different trials were run. A view of the mesh is given in Figure 4. (This is not the view of the whole mesh but of only part of the mesh.) A close-up view of the mesh is given in Figure 6. Because the Gauss quadrature is used rather than the Gauss–Lobatto, the close-up view demonstrates how the grid points do not extend to the edge of the subdomains.

Table 1. Parameters used in the numerical simulation of flow around a circular cylinder.

Inlet Height:	1 m
Cylinder Radius:	0.05 m
Mach #:	0.2
Temperature:	300 K
Density:	1.2 kg/m^3
Polynomial Degree:	12
Scheme:	Second Order Runga–Kutta, $\Delta t = 10^{-4}$.

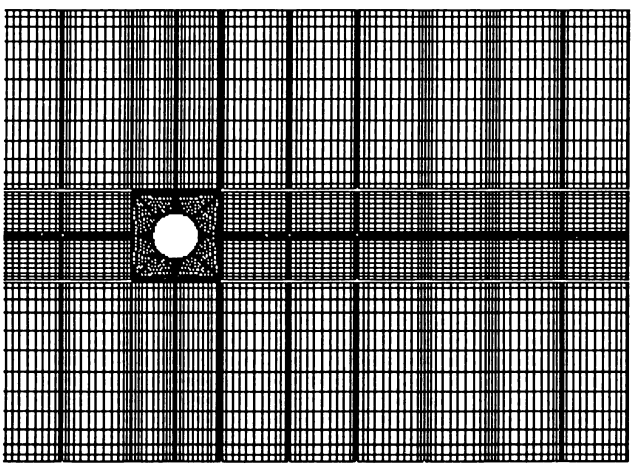

Fig. 5. Partial view of the mesh for flow around a circular cylinder.

The first trial was started using a symmetric initial condition. The initial condition that was used came from steady-state incompressible flow around a cylinder.

This trial was used to insure that the implementation was consistent with other results and to check that the flow remained symmetric. The level curves of the density and mach numbers can be found in Figures 7 and 8.

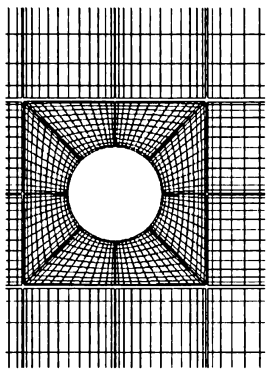

Fig. 6. Close-up view of the mesh for flow around a circular cylinder.

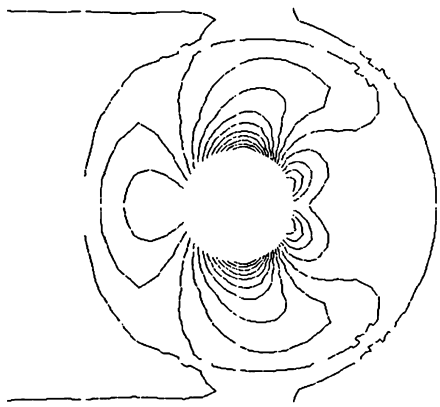

Fig. 7. Density after 5,000 time steps for symmetric initial condition.

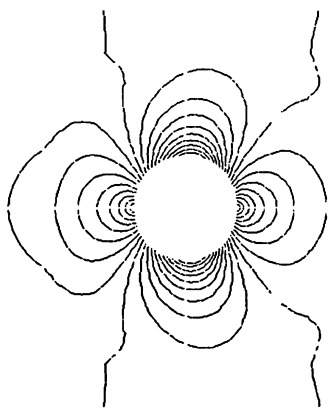

Fig. 8. Mach number after 5,000 time steps for symmetric initial condition.

The second trial was run for a nonsymmetric initial condition. In this second trial the initial condition was based on the steady-state incompressible flow around a circular cylinder. However, the velocity in the y direction in the first quadrant (with respect to the center of the cylinder) was taken to be the negative of the true velocity. The numerical trial was then run to examine the steady state of this new flow.

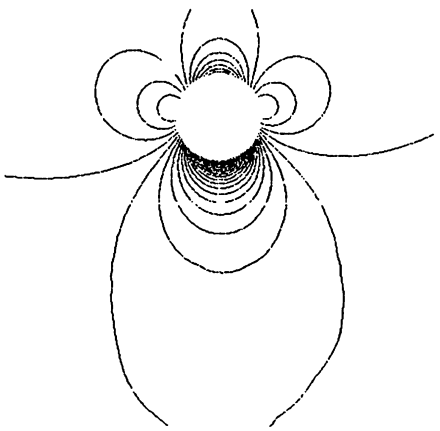

Fig. 9. Density after 200,000 time steps for non-symmetric initial condition.

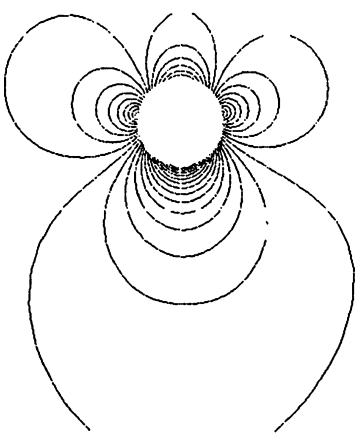

Fig. 10. Mach number after 200,000 time steps for non-symmetric initial condition.

The small value for the time step used in these problems was chosen to reduce errors associated with the time stepping. This was done in order to more closely examine the properties of the spatial approximation. Numerical experiments have been conducted with varying time steps. No theoretical results have been found yet, but the CFL condition of the scheme appears to be consistent with those given by Hesthaven [10, 8].

4. 'CONCLUSIONS

A spectral element approximation for the Euler equations describing inviscid compressible flow is given. The method is similar to the discontinuous Galerkin method. The computational domain is subdivided into separate subdomains, and a high-order polynomial approximation is constructed within each subdomain.

The variational form and the use of the Legendre–Gauss quadrature allow for an high-order approximation, and the influence between subdomains is accomplished through a flux splitting scheme on the subdomain interfaces. The scheme is conservative. Moreover, the numerical results are similar to thos presented by Kopriva [11, 12]. The convergence rates are slightly faster, but the accuracy of the method is reduced for deformed subdomains.

The principal advantage of the scheme is in its simplicity. While Kopriva's scheme requires the translation of the conserved variables over three different grids, only one grid is used for the discontinuous-Galerkin scheme, and the scheme is easier to implement. Moreover, the use of only one grid reduces the operation count. The $O(N^3)$ operation of translating to the different grids is not required for the discontinuous-Galerkin scheme.

ACKNOWLEDGEMENTS

I would like to thank David Kopriva. His discussions and help have been greatly appreciated and made much of this work possible.

(Received April 8, 1998.)

REFERENCES

[1] F. Bassi and S. Rebay: A high–order accurate discontinuous finite element method for the numerical solution of the compressible Navier–Stokes equations. J. Comput. Phys. *131* (1997), 267–279, 1997.

[2] B. Cockburn and C. W. Shu: TVB Runga–Kutta local projection discontinuous Galerkin finite–element method for conservation laws II: General framework. Math. Comp. *52* (1989).

[3] B. Cockburn and C. W. Shu: TVB Runga–Kutta local projection discontinuous Galerkin finite–element method for conservation laws III: One dimensional systems. J. Comput. Phys. *84* (1989), 90.

[4] B. Cockburn and C. W. Shu: TVB Runga–Kutta local projection discontinuous Galerkin finite–element method for conservation laws IV: The multidimensional case. Math. Comp. *54* (1990).

[5] R. Courant and K. O. Friedrichs: Supersonic Flow and Shock Waves. Applied Mathematical Sciences. Springer–Verlag, New York 1948.

[6] W. J. Gordon and C. A. Hall: Transfinite element methods: Blending–function interpolation over arbitrary curved element domains. Numer. Math. *21* (1973), 109–129.

[7] A. Harten, P. D. Lax and B. Van Leer: On upstream differencing and Godunov–type schemes for hyperbolic conservation laws. SIAM Review *25* (1983), 1, 35–61.

[8] J. S. Hesthaven: A stable penalty method for the compressible Navier–Stokes equations II: One dimensional domain decomposition schemes, to appear.

[9] J.S. Hesthaven: A stable penalty method for the compressible Navier–Stokes equations III: Multi dimensional domain decomposition schemes, to appear.
[10] J.S. Hesthaven and D. Gottlieb: A stable penalty method for the compressible Navier–Stokes equations. I. Open boundary conditions. SIAM J. Sci. Statist. Comput *17* (1996), 3, 579–612.
[11] D.A. Kopriva: A Conservative Staggered Grid Chebychev Multi-Domain Method for Compressible Flows. II: A Semi-Structured Method. NASA Contractor Report ICASE Report No. 96-15, ICASE, NASA Langley Research Center, 1996.
[12] D.A. Kopriva and J.H. Kolias: A conservative staggered grid Chebychev multi-domain method for compressible flows. J. Comput. Phys. *125* (1996), 1, 244–261.
[13] C. Rumsey, B. van Leer and P.L. Roe: A multidimensional flux function with applications to the Euler and Navier–Stokes equations. J. Comput. Phys. *105* (1993), 306–323.

Kelly Black, Department of Mathematics, University of New Hampshire, Durham, NH 03824. U.S.A.
e-mail: black@vidalia.unh.edu